Continental Shelf Research 243 (2022) 104752

Contents lists available at ScienceDirect

Continental Shelf Research

journal homepage: www.elsevier.com/locate/csr

Impacts of glacier and sea ice melt on methane pathways on the Northeast Greenland shelf

Josefa Verdugo [a,b,*], Ellen Damm [c], Janin Schaffer [a], Dorothea Bauch [d,e], Hanno Meyer [c], Jan Kaiser [f]

[a] Alfred-Wegener-Institute, Helmholtz-Centre for Polar and Marine Research, Bremerhaven, 27570, Germany
[b] University of Bremen, Faculty 2 Biology/Chemistry, Bremen, 28359, Germany
[c] Alfred-Wegener-Institute, Helmholtz Centre for Polar and Marine Research, Potsdam, 14473, Germany
[d] Leibniz Laboratory for Radiometric Dating and Stable Isotope Research, Kiel University, Kiel, 24118, Germany
[e] GEOMAR Helmholtz Centre for Ocean Research, Kiel, 24148, Germany
[f] Centre for Ocean and Atmospheric Sciences, School of Environmental Sciences, University of East Anglia, Norwich, NR4 7TJ, United Kingdom

A B S T R A C T

Global warming has led to a sharp decrease in Arctic summer sea ice extent and a dramatic ice mass loss of the Greenland Ice Sheet over the past three decades. The Northeast Greenland continental shelf is a site of intense water mass transformation involving both sea ice processes and glacier dynamics. The Arctic shelf waters are considered to be a net source of atmospheric methane (CH_4); however, the effect of glacier and sea ice melt on oceanic CH_4 concentrations still needs to be investigated. To better understand the effect of meltwater on the CH_4 budget of the ocean, our study constrains the CH_4 pathways by following changes in water mass properties and infers potential CH_4 sources and sinks. Based on measurements of concentration and carbon isotope delta ($\delta^{13}C$) of CH_4, the water mass tracer $\delta^{18}O$ (H_2O) and physical properties of the water masses, we detected CH_4 excess in surface waters, which we attribute to brine release during sea ice formation. We show that this CH_4 excess is sustained throughout the melt season, due to a freshwater lid formed at the ocean surface. The meltwater hardly alters the CH_4 excess, but enhances water stratification, which, in turn, restricts the sea-to-air flux. The CH_4 excess is subject to mixing with surrounding shelf waters influenced by basal glacial meltwater discharge. We suggest that the CH_4 excess of Northeast Greenland continental shelf waters is redistributed in the marine environment, while CH_4 emission to the atmosphere is limited to regions not covered by sea ice.

1. Introduction

Arctic Amplification of global warming has led to a sharp decrease in Arctic summer sea ice extent, ice thickness, and volume since 1979 (Stroeve and Notz, 2018). Decreasing by about 44% over the last four decades (Perovich et al., 2020), summer sea ice is currently shifting from multi-year ice to thin first-year ice (Kwok, 2018). As summer sea ice extent continues to diminish, the decreasing capacity of sea ice to prevent exchange of gases may influence the cycling of methane, CH_4 (Parmentier et al., 2013), a potent greenhouse gas contributing to global warming (IPCC, 2021). Recent observations show that the Arctic continental shelves are super-saturated in CH_4: in particular on the continental shelves off the coast of Greenland (Crabeck et al., 2014; Kitidis et al., 2010), Spitsbergen (Damm et al., 2005; Silyakova et al., 2020), and on the East Siberian shelf (Shakhova et al., 2005; Vinogradova et al., 2022). However, the amount of CH_4 released to the atmosphere at the sea-air interface is not just triggered by the amount of super-saturation but also by pronounced seasonal water transformations in Arctic regions (Damm et al., 2018, 2021). In summer, water stratification favours lateral CH_4 transport in the water column (Damm et al., 2005, 2021; Gentz et al., 2014; Silyakova et al., 2020), promoting CH_4 oxidation that ultimately reduces the amount of CH_4 that escapes from the ocean surface into the atmosphere (Mau et al., 2013, 2017). In contrast, cooling in autumn favours convection and CH_4 release into the atmosphere in ice-free Arctic regions (Damm et al., 2021), whereas in ice-covered regions, CH_4 is accumulated and stored in the winter mixed layer (Damm et al., 2015) and is available for further microbial oxidation. On continental shelves adjacent to marine-terminating glaciers at the coast, additional meltwater from glacier melting is added into the ocean, enhancing the stratification of the water column but also inhibiting the sea-to-air flux of CH_4. Hence, Arctic shelf processes affect the ultimate fate of CH_4.

Our study is focused on the Northeast Greenland (NEG) continental shelf (Fig. 1), a site of intense water mass transformations. The properties of Polar Surface Water (PSW) are influenced by sea ice freeze and melt cycles (Budéus and Schneider, 1995), as well as surface runoff from

* Corresponding author. Alfred-Wegener-Institute, Helmholtz-Centre for Polar and Marine Research, Bremerhaven, 27570, Germany.
E-mail address: maria.josefa.verdugo@awi.de (J. Verdugo).

https://doi.org/10.1016/j.csr.2022.104752
Received 1 February 2021; Received in revised form 6 May 2022; Accepted 8 May 2022
Available online 13 May 2022

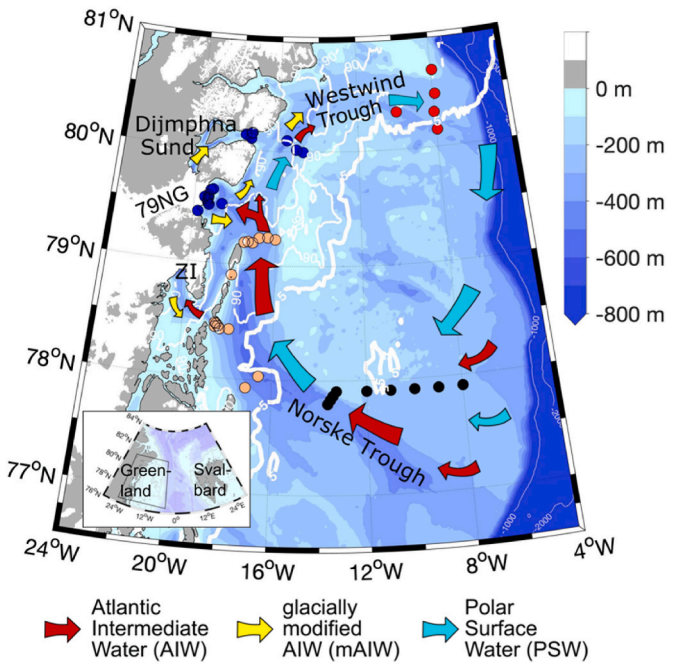

Fig. 1. The Northeast Greenland (NEG) continental shelf with coloured dots showing the CTD stations, the CH_4 and $\delta^{18}O$ sampling in certain geographic areas. Black dots show stations on the Norske Trough, brown dots the islands and outlet of ZI, blue dots the outlet of the 79NG to the trough system south of the Dijmphna Sund mouth, and red dots the Westwind Trough. The colour bar shows the bathymetry of the region. The arrows sketch the circulation pattern relevant for the transport of the water masses. We highlight the locations of the Nioghalvfjerdsfjorden glacier (79NG) and Zachariae Isstrøm (ZI). White lines mark the extent of the sea ice cover on September 20, 2017 (Spreen et al., 2008) with the thick and thin contour lines representing 5v% and 90% sea ice concentration, respectively. The inset in the left corner shows the location of the NEG area.

glaciers, subglacial meltwater runoff (Huhn et al., 2021), frontal meltwater runoff, and submarine melting of icebergs (Enderlin et al., 2016). Subglacial discharge plumes are sometimes observed at the ocean surface during the summer season, as reported in a fjord system in central West Greenland (Mankoff et al., 2016). In our study region, subglacial discharge plumes have also been observed during late summer (Fig. 2a). Below PSW, sea ice-influenced Knee Water (KW) is exported from the Arctic Ocean to the inner shelf. The inflow of relatively warm Atlantic Intermediate Water (AIW) to the inner shelf drives glacial basal melt (Schaffer et al., 2017, 2020). The mixture of subglacial runoff draining down to the grounding line, glacial basal meltwater and AIW forms glacially modified AIW (mAIW). Hence, the impact of glacier and sea-ice melt on CH_4 pathways on the NEG continental shelf can be traced by following the signal of the water mass transformations. These circumstances allow us to understand the oceanic CH_4 budget in waters influenced by meltwater.

Here, we offer new insights on the impact of sea ice and glacial ice dynamics on CH_4 pathways during the melting peak at the summer-autumn transition when sea ice, land-fast ice, and glacial ice discharge the largest amounts of freshwater into the shelf waters. Using combined analysis of water temperature and salinity, the concentration and carbon isotope delta ($\delta^{13}C$) of CH_4, and $\delta^{18}O(H_2O)$, we provide a detailed analysis of the impact of water mass transformations on CH_4 pathways on the shelf. We infer how sea ice formation and melt affect the CH_4 budget of PSW and KW. We discuss the impact of surface and basal meltwater discharge on potential sea-to-air emissions of CH_4 and the oceanic CH_4 budget. In addition, we refer to the biogeochemical and physical processes that affect CH_4 in AIW and its subsequent mixing with basal glacial meltwater. By this, we identify marine transport pathways of CH_4 and highlight its sources and main sinks in NEG continental shelf waters.

2. Regional setting

The NEG continental shelf region extends more than 300 km from the coastline, representing the broadest shelf along the Greenland margin. Large areas of the shelf are covered by land-fast ice and drifting sea ice exported from the central Arctic Ocean further offshore. Land-fast ice has broken up regularly in the summers since 2000 (Sneed and Hamilton, 2016) and since then it mainly consists of first-year fast ice (Sneed and Hamilton, 2016). Both types of sea ice feature large areas of the ocean surface on the continental shelf throughout the year. Subglacial runoff and basal meltwater occur mainly from the Nioghalvfjerdsfjorden glacier (79NG), the Zachariae Isstrøm glacier (ZI) and Storstrømmen glacier, currently draining 12% (320 000 km^2) of the Greenland Ice Sheet via the Northeast Greenland Ice Stream (Rignot and Mouginot, 2012). The 80 km long and 20 km wide floating 79NG tongue covers an entire fjord. The glacier tongue widens to a 30 km wide main calving front eastwards and drains additionally northwards into the Dijmphna Sund, where it forms an 8 km long calving front (Mayer et al., 2000) (Fig. 1). In contrast, the ZI glacier had lost all of its floating ice tongues by spring 2015 (Mouginot et al., 2015). Both glaciers interact with warm ocean waters causing substantial basal meltwater discharge (Schaffer et al., 2020; Wilson et al., 2017). Former glacial activities shaped the prominent cross-shelf trough system at the seafloor of the NEG continental shelf (Fig. 1, Arndt et al., 2015). These bathymetric features enable the transport of warm (i.e., above 1 °C) AIW into the fjord. AIW originates mainly from recirculating waters in the Fram Strait, and it is transported from the shelf break via the Norske Trough towards the inner shelf (Schaffer et al., 2017) and below 79NG (Schaffer et al., 2020). The oceanic heat drives basal melting along the underside of the glacier tongue. Subsequently, glacial meltwater mixes with AIW inside the subglacial cavity. At the calving front, this glacially modified AIW

Fig. 2. Photo of the 79NG at the Northeast Greenland region showing (a) subglacial meltwater plume, (b) and (c) surface runoff during PS100. Photo credit: Fig. 2a and c: Dennis Köhler and Fig. 2b: Janin Schaffer.

(mAIW, which is on average 0.9 °C cooler than the inflowing AIW) flows out of the cavity (Schaffer et al., 2020). MAIW water mass mixes with cold and saline brine-enriched KW (Bourke et al., 1987; Budéus and Schneider, 1995), both having the same density class. On top of KW, cold PSW is confined. In contrast to KW that is exported from the Arctic Ocean, PSW forms locally on the NEG continental shelf (Budéus and Schneider, 1995). In summer, PSW becomes fresher and stratified on top, and the meltwater discharge contributes to this Meltwater Layer (MWL), while underneath a residual Winter Mixed Layer (WML) remains sustained. The clockwise circulation transports meltwater around the NEG continental shelf, while lateral water exchange and vertical mixing modify the water mass properties (Fig. 1, Bourke et al., 1987; Budéus and Schneider, 1995).

3. Methods

Sampling was carried out on the NEG continental shelf onboard RV *Polarstern* expedition PS109 from 12 September to October 14, 2017 (Fig. 1). Vertical profiles of conductivity, temperature, fluorescence, and oxygen concentration were measured daily with a shipboard Sea-Bird Scientific SBE911plus CTD (Conductivity Temperature Depth profiler), integrated into a SBE32 Carousel Water Sampler with 24 Niskin bottles of 12 L each (Kanzow and Rohardt, 2017). The CTD data were post-processed according to standard post-cruise processing and calibration procedures (Rohardt, 2017).

3.1. Methane concentration and isotope ratio analyses

Discrete seawater samples were collected for the analysis of CH_4 concentrations and carbon isotope delta, $\delta^{13}C$, at different depths throughout the water column using the CTD water sampling carousel. Samples were taken in a procedure that prevented air bubbles during sampling and filled in 120 mL glass vials, using gas-impermeable *Tygon* tubing, and were sealed directly with rubber stoppers and crimped with aluminium caps. Duplicate samples for CH_4 concentrations were taken at each depth and subsequently analysed onboard. A 5 mL headspace was created by the addition of N_2 gas into the vials, and then equilibrated for 1 h at room temperature. Afterwards, a 1.5 mL gas sample was taken from the headspace and injected into a gas chromatograph (Agilent GC 7890B) with a Flame Ionization Detector (FID). For gas chromatographic separation, a 12 µm molecular sieve 5 Å column (30 m length, 0.32 mm wide) was used. The GC was operated isothermally (60 °C) and the FID was held at 200 °C (Damm et al., 2018). Four sets of gas mixtures (4.99, 10.00, 24.97, and 50.09 µmol mol^{-1} CH_4 in N_2) were used for calibration. The relative standard deviation of duplicate analyses was 5%. The CH_4 saturation was calculated from the CH_4 equilibrium concentration at in situ temperature and practical salinity values (using the processed CTD 'bottle-file' data) following (Wiesenburg and Guinasso Jr, 1979) and using an atmospheric CH_4 mole fraction of 1.91 µmol mol^{-1}, corresponding to the monthly mean for June 2017 at Zeppelin Station, Spitsbergen (NOAA Global sampling networks, http://www.esrl.noaa.gov, last access: July 6, 2020). CH_4 equilibrium concentrations ranged between 3.8 and 4.1 nmol L^{-1} for $31 \leq S \leq 35$, temperatures between local freezing point and 0 °C, and a barometric pressure of 1013.25 Pa (1 atm).

An additional 120 mL–glass bottle was taken for determining $\delta^{13}C$ and those samples were collected following the same procedure as for CH_4 concentrations. The samples were kept in a 4 °C cold dark room. At the home laboratory at the Alfred-Wegener-Institute Helmholtz Centre for Polar and Marine Research (AWI), a headspace was created by injecting 25 mL of N_2 gas into each vial and letting water and gas phases equilibrate for 1 h at room temperature. Afterwards, 20 mL of gas were taken from the headspace and injected into a PreCon device coupled to a Thermo Finnigan Delta plus XP mass spectrometer. Within the PreCon, the extracted gas was purged and trapped to pre-concentrate the sample. $^{13}C/^{12}C$ isotope ratios are reported as δ-values relative to the Vienna Pee Dee Belemnite (VPDB) standard.

3.2. Water mass fraction analyses

Discrete seawater samples for the $^{18}O/^{16}O$ isotope delta of the water, $\delta^{18}O(H_2O)$, were collected in screw cap glass bottles using the CTD water sampling carousel at the same depths as for the CH_4 concentration and $\delta^{13}C$ samples. The $\delta^{18}O(H_2O)$ values were measured in the Isotope Laboratory of the AWI Research Unit Potsdam. For the online determination of hydrogen and oxygen isotopic composition, a Finnigan MAT Delta S mass spectrometer with two equilibration units was used. The external errors of long-term standard measurements for hydrogen ($^2H/^1H$) and oxygen ($^{18}O/^{16}O$) isotope ratios are better than 0.8‰ and 0.10‰, respectively (Meyer et al., 2000). Only $\delta^{18}O$ values are used here because the δ^2H are highly correlated to $\delta^{18}O$ and do not provide additional information.

Water mass fractions are calculated using temperature, salinity, and $\delta^{18}O$ for fractions of marine water (f_{mar}), meteoric water (f_{met}), sea ice melt (f_{sim}), and basal melt (f_{bas}) by solving the following equations (see Table 1 for the endmember values of the different water masses):

$$f_{sim} + f_{met} + f_{mar} + f_{bas} = 1 \quad (1)$$

$$f_{sim}\delta_{sim} + f_{met}\delta_{met} + f_{bas}\delta_{bas} + f_{mar}\delta_{mar} = \delta_{sample} \quad (2)$$

$$f_{sim}S_{sim} + f_{met}S_{met} + f_{bas}S_{bas} + f_{mar}S_{mar} = S_{sample} \quad (3)$$

$$f_{sim}T_{sim} + f_{met}T_{met} + f_{bas}T_{bas} + f_{mar}T_{mar} = T_{sample} \quad (4)$$

where f_{sim}, f_{met} f_{mar}, and f_{bas} are the fractions of sea ice meltwater, meteoric water, marine water (AIW), and basal meltwater in a water parcel, respectively. The corresponding $\delta^{18}O(H_2O)$ values, salinities and temperatures are designated with the symbols δ, S and T.

$\delta^{18}O(H_2O)$ is a conservative property that is altered by fractionation due to phase transitions only. Likewise, S and T can be treated as conservative properties in the ocean interior and ice-covered surface waters, for which heat exchange with the atmosphere, precipitation and evaporation can be neglected. Uncertainties in the calculated water mass fractions f are about 1% and depend on measurement precision and uncertainties in the values of the chosen endmembers. The net sea ice formation (formation exceeding melting) will generate a negative sea ice meltwater fraction ($f_{sim} < 0$) since freezing withdraws water from the liquid ocean.

A distinct selection of endmember values is required for each region (Bauch et al., 2010). We assume marine and meteoric waters to originate in first order from the central Arctic Ocean and endmember values were chosen according to Arctic halocline waters exported through Fram Strait in the East Greenland Current and to reflect accumulated meteoric and sea ice components within the Arctic Basin. Therefore, the marine source was chosen according to the Atlantic Layer in the southern Nansen Basin ($T_{mar} = 2$ °C, $S_{mar} = 34.96$, $\delta_{mar} = 0.3$‰). The mean δ value of river-runoff within the Arctic Ocean of −20‰ (Bauch et al., 1995; Ekwurzel et al., 2001) is taken as meteoric water endmember δ_{met},

Table 1
Endmember values used in a quaternary mixing between Atlantic Intermediate Water (marine water), surface melt (meteoric water), basal melt, and sea ice melt.

Endmember	$\delta^{18}O(H_2O)$/‰, rel. to VSMOW	Salinity S	Temperature (°C)
Sea ice meltwater	0.60	4	−82.71
Meteoric water	−20.00	0	0
Marine water	0.12	34.96	2.0
Basal meltwater	−37.00[a]	0	−100.37

Uncertainties for $\delta^{18}O(H_2O)$, salinity, and temperature are 0.10, 0.02, and 0.02, respectively.

[a] Based on Greenland Ice Core Project (GRIP) records and Eemian ice.

with $S_{met} = 0$ and $T_{met} = 0$ °C. For basal meltwater, we used $\delta_{bas.} = (-37 \pm 5)$ ‰ (based on the GRIP ice core), with $S_{bas} = 0$ and $T_{bas} = (-100 \pm 6)$ °C, at a depth of 500 m. The latter value incorporates the latent heat of ice melting, and assumes a far-field ice temperature of (-38 ± 12) °C (again corresponding to the GRIP ice core). For the sea ice endmember, we used $\delta_{sim} = -1.7$‰, based on average surface water $\delta = -3.8$‰ and an isotopic fractionation of +2.1‰ during sea ice formation (Bauch et al., 1995), $S_{sim} = 4$ and $T_{sim} = (-83 \pm 3)$ °C. Just as for glacial ice, the latter value incorporates the latent heat of ice melting, but in this case uses an ice temperature of (−5±5) °C.

4. Results

We combined the physical data (potential density anomaly σ_θ, temperature T, salinity S, $\delta^{18}O(H_2O)$) with the biogeochemical data (CH_4 concentration, saturation, $\delta^{13}C$) to follow CH_4 pathways directly related to the water masses locally formed or transported towards the NEG continental shelf in the early autumn 2017. The properties of the water masses and the CH_4 signal therein are modified on the continental shelf. To trace those changes, we separated the trough system (with its anticyclonic shelf circulation) into four regions (Fig. 1). From south to north, the first region covers the northern part of the Norske Trough, the second the "islands and outlet of ZI" between 78° N and 79° N, the third the outlet of the 79NG to the trough system south of the Dijmphna Sund mouth, and the fourth the Westwind Trough. We found distinctive CH_4 signals (CH_4 concentration and $\delta^{13}C$) in each water mass (Fig. 3 and Fig. 4). In the following, we characterise each water mass in detail.

4.1. Polar Surface Water (PSW)

The cold and fresh PSW is locally formed on the shelf. This sea ice-influenced water mass covered the upper 75 m of the water column on the continental shelf. Based on the definition by (Bourke et al., 1987), the lower boundary of PSW is given by $\sigma_\theta < 26.25$ kg m^{-3}, with $\theta < 0$ °C and $S < 32$. Furthermore, in summer the MWL is formed on top of WML, separating PSW into two layers (Fig. 5).

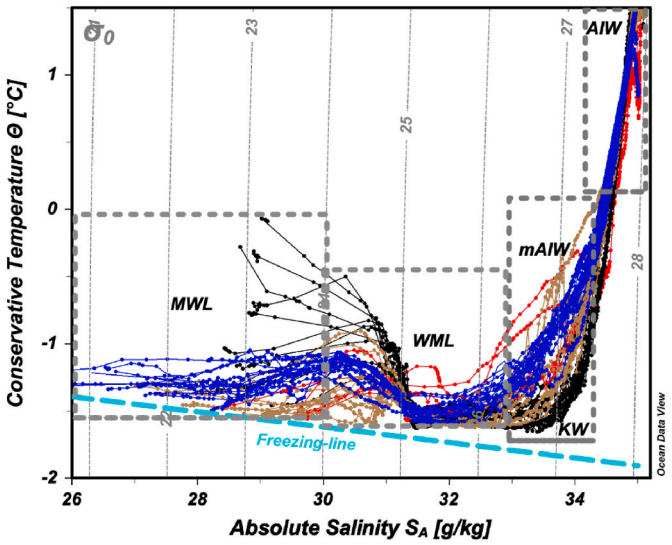

Fig. 3. T-S diagram for all sampling stations on the NEG continental shelf during the PS109 expedition. Colours represent different geographic areas (see Fig. 1). We highlight the presence of the Meltwater Layer (MWL), the Winter Mixed Layer (WML), the Knee Water (KW), the modified Atlantic Intermediate Water (mAIW), and Atlantic Intermediate Water (AIW). The dashed line indicates the salinity dependence of the freezing temperature and the grey lines indicate the potential density (σ_θ). Figure was made in ODV (Schlitzer, 2020).

4.1.1. Meltwater layer (MWL)

The MWL is defined by $\sigma_\theta < 24.0$ kg m^{-3} with $\theta > -1.57$ °C and $S < 30.0$ (Figs. 3 and 5). This freshwater layer contributed to a stratified and stable upper water column at stations in front of the 79NG and the (inner) Dijmphna Sund shown by the Brunt-Väisälä (buoyancy) frequency (Fig. 5c (Gill, 1982)). In Dijmphna Sund and at the stations near the Nioghalvfjerdsfjorden glacier (79NG), the MWL was fresher than further offshore (Fig. 5b). The CH_4 concentrations ranged from 3.8 nmol L^{-1} to 5.4 nmol L^{-1} (average: 4.7 nmol L^{-1}), corresponding to under and super-saturation between 94%, and 134% (average: 116%), respectively, relative to the atmospheric equilibrium concentration (Fig. 5d and 5e). The $\delta^{13}C$ values varied between −49.7‰ and −42.9‰. Compared with the atmospheric regional background signature of −47.8‰ (Zeppelin Station, Spitsbergen), adjusted for the equilibrium isotope fractionation between gaseous and dissolved CH_4 of 0.3‰ (Fuex, 1980), i.e., −47.5‰, values deviate from the atmospheric background signature (Fig. 4). The $\delta^{18}O(H_2O)$ values varied between −4.1‰ and −3.5‰, and in combination with salinity points towards the contribution of local meteoric water in this region (Figs. 5g and 6).

4.1.2. Winter mixed layer (WML)

WML is confined below the MWL. This water mass is defined by 24 kg m^{-3} < σ_θ < 26.25 kg m^{-3} with $\theta > -1.6$ °C, and $S > 30$ (Fig. 2). The minimum temperatures were found deeper than 50 m in the water column. Below 50 m it remained at temperatures of about −1.5 °C down to 80–90 m depth (Fig. 5a). The salinity increased with water depth (Fig. 5b). The thickness of WML decreased from the Norske Trough towards the Westwind Trough. CH_4 concentrations ranged between 4.2 nmol L^{-1} and 5.6 nmol L^{-1} (average: 5.0 nmol L^{-1}) corresponding to saturations between 105% and 138% (average: 123%), i.e., WML is CH_4 super-saturated, relative to the atmospheric equilibrium concentration (Fig. 5e). The $\delta^{13}C$ values ranged between −48.0‰ and −39.8‰, similar to the $\delta^{13}C$ values found in the MWL (Fig. 5f). The $\delta^{18}O(H_2O)$ values varied between −3.5‰ and −2.2‰, and in combination with salinity reflect the influence of brine release during sea ice formation (Figs. 5g and 6).

4.2. Knee Water (KW)

Exported from the Arctic Ocean, KW is localised underneath WML (Budéus and Schneider, 1995). This water mass can be separated from PSW by an intermediate temperature increase (as small as 0.1 °C, i.e., temperatures remaining close to the freezing point) while salinities increase continuously with depth (Figs. 3 and 5a and b). We computed the lower boundary of KW based on a vertical temperature difference larger than 0.2 °C relative to 10 m water depth (at depth below 50 m). The depth of KW gets shallower toward the Westwind Trough (Fig. 5). CH_4 concentrations ranged between 3.2 nmol L^{-1} and 5.4 nmol L^{-1} (average: 4.5 nmol L^{-1}), corresponding to saturation levels between 88% and 135% (average: 114%). The $\delta^{13}C$ values ranged between −46.2‰ and −37.6‰. Hence, relative to WML, KW contains slightly lower CH_4 concentration, while the $\delta^{13}C$ values are higher (Fig. 5d and 5f). The $\delta^{18}O(H_2O)$ values varied between −2.41‰ and −0.55‰, and in combination with salinity indicate the influence of brine release during sea ice formation (Figs. 5g and 6).

4.3. Glacially modified Atlantic Intermediate Water (mAIW)

Glacially modified Atlantic Intermediate Water (mAIW) formed at the coast by mixing of AIW with basal meltwater and subglacial runoff from the 79NG and ZI is advected onto the shelf at depth below PSW. Following Schaffer et al. (2020), mAIW is defined by a density range of 26.25 kg m^{-3} < σ_θ < 27.75 kg m^{-3}, i.e., covering partly the density range of KW (Figs. 2 and 5). In comparison to KW, mAIW is warmer at the same salinities (Fig. 3). We pose that a mixture of KW (advected from Norske Trough) and mAIW (advected onto the shelf from the 79NG and

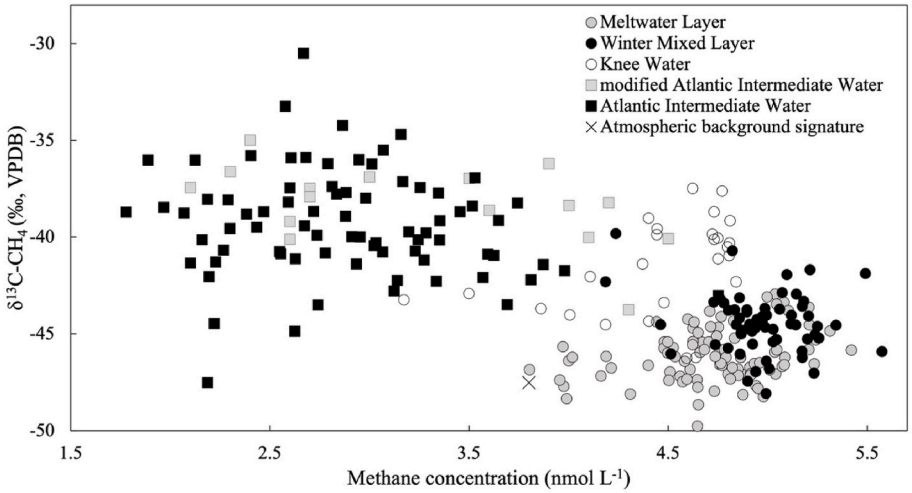

Fig. 4. The $\delta^{13}C$ over the CH_4 concentration in different water masses on the NEG continental shelf. The cross indicates both the atmospheric equilibrium concentration (3.8 nmol L^{-1}) and the equilibrium $\delta^{13}C$ of dissolved atmospheric CH_4 of −47.5‰ which corresponds to the regional atmospheric $\delta^{13}C$ value of −47.8‰ (White et al., 2018) corrected for the equilibrium isotopic fractionation effect (0.3‰: Fuex, 1980).

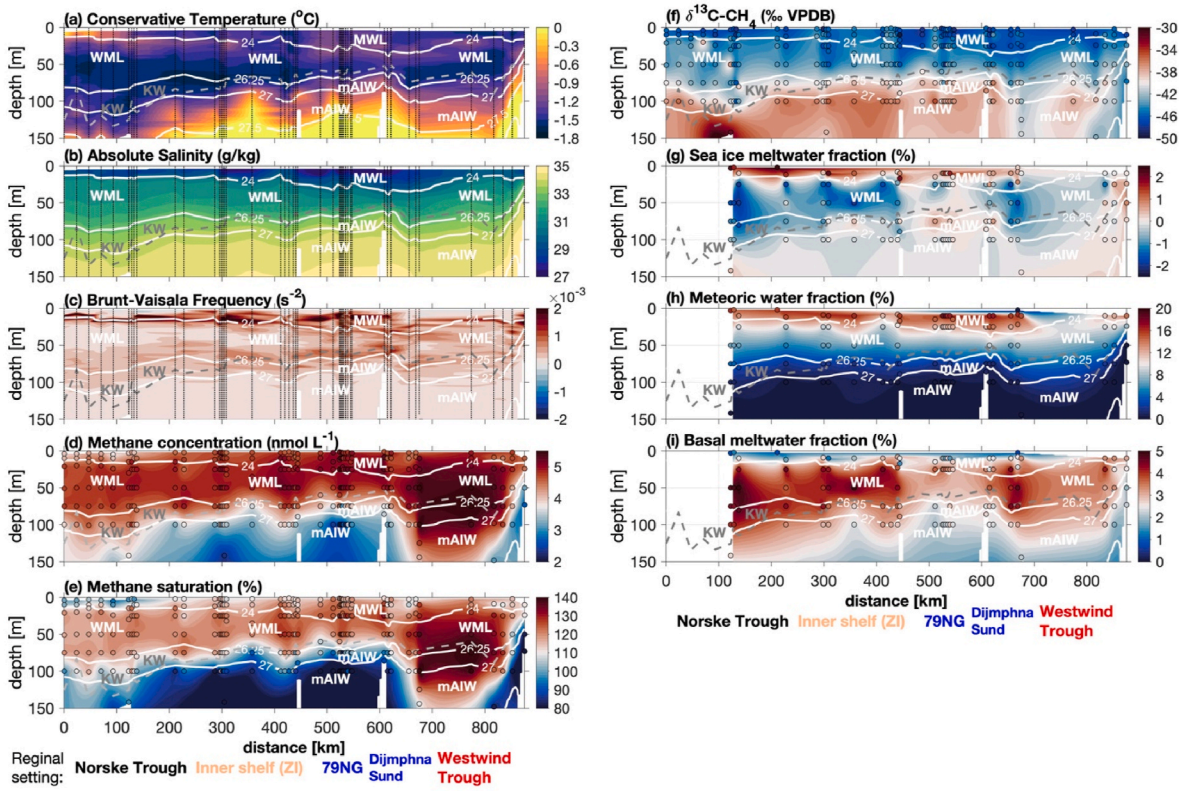

Fig. 5. Vertical distribution of several parameters in the upper 150 m on the NEG shelf, including the Meltwater Layer (MWL) on top, the Winter Mixed Layer (WML), Knee Water (KW), and the modified Atlantic Intermediate Water (mAIW). Transects follow the anticyclonic shelf circulation starting close to the shelf in Norske Trough (South) following the trough system towards the inner shelf including the 79NG and Dijmphna Sund and finishing at the mouth of Westwind Trough (Fig. 1). (a) Conservative temperature, (b) Absolute salinity, (c) Brunt-Väisälä (buoyancy) frequency, (d) CH_4 concentration, (e) CH_4 saturation, (f) $\delta^{13}C$, (g) sea ice meltwater fraction (f_{sim}), and (h) meteoric water fraction (f_{met}), and (i) basal meltwater fraction (f_{bas}). There are no $\delta^{18}O(H_2O)$ data available for Norske Trough. White lines are depicted isopycnals used to separate water masses. The grey dashed line marks the lower boundary of KW computed based on a vertical temperature difference larger than 0.2 °C relative to 10 m water depth (at depth below 50 m). Fig. 4a–i were made in Matlab R2020b. For panels a–c data were linear interpolated, horizontally (along the section) and vertically (between depth levels), on a regular grid. For panels, d-i a natural neighbour interpolation was used.

ZI) is transported with the anti-cyclonic shelf circulation into Westwind Trough (Figs. 1 and 3). CH_4 concentrations in mAIW varied from 2.0 nmol L^{-1} to 4.5 nmol L^{-1}. The highest concentrations were found in the Westwind Trough at the interface between KW and mAIW, reflecting mixing between both water masses. The $\delta^{13}C$ values ranged between −43.7‰ and −34.9‰ (Fig. 4). Relative to values in KW, mAIW showed lower CH_4 concentration, while the $\delta^{13}C$ values were similar, indicative of CH_4 dilution via mixing. The $\delta^{18}O(H_2O)$ values varied between

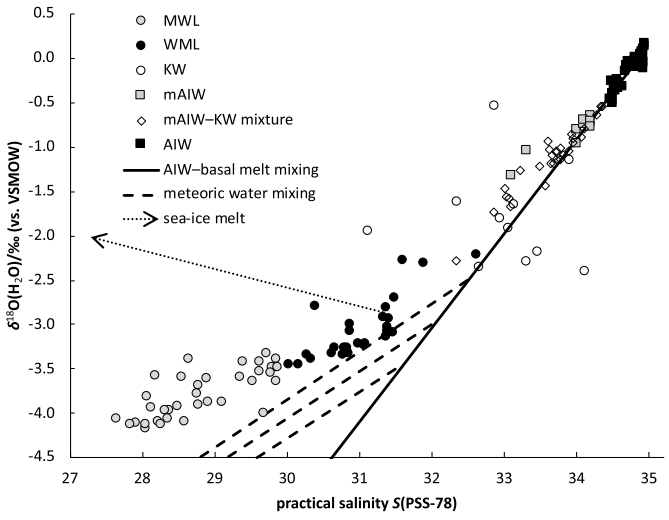

Fig. 6. $\delta^{18}O(H_2O)$ values versus salinity in all water masses. The solid line represents mixing between marine water and basal meltwater (see also Table 1). An array of three dashed lines indicates the effect of mixing subsurface waters with the meteoric water endmember. The dashed line with an arrow illustrates what effect the addition of sea ice melt would have. Atlantic Intermediate Water (AIW) values scatter close to the high salinity endmember indicating that AIW contains little basal meltwater and meteoric waters. During the circulation on the continental shelf, mixing between AIW and glacial basal meltwater occurs as well as sea ice formation, i.e., modified Atlantic Intermediate Water (mAIW) scatter around the solid mixing line, but at lower salinities and $\delta^{18}O$ values. KW (Knee Water) and winter mixed layer (WML) deviate the most due to the influence of sea ice formation and melt. Meltwater layer (MWL) values are affected by a combination of meteoric water addition and summer sea ice melt.

−1.34‰ and −0.64‰, reflecting a small contribution of meltwater (Figs. 5i and 6).

4.4. Atlantic intermediate water (AIW)

AIW was found at depths below 200 m. Based on Budéus and Schneider (1995), AIW is defined by $\sigma_\theta > 27.7$ kg m^{-3}, with $\theta > 0$ °C and $S > 34.4$ (Fig. 3). CH_4 concentrations ranged from 1.8 nmol L^{-1} to 4.0 nmol L^{-1} (Fig. 4). One exception was observed at station 42 (outside Djimphna Sund, 80° N, 15.1° W), at 203 m depth with 4.7 nmol L^{-1}, which reflects methane resuspension at the water-sediments interface. The $\delta^{13}C$ values ranged between −47.5‰ and −30.5‰ (Fig. 4). The CH_4 concentrations and the $\delta^{13}C$ values were similar to those found in mAIW in stations in front of the 79NG. However, relative to PSW, CH_4 concentration in AIW was lower and the $\delta^{13}C$ values were higher (Fig. 4). The $\delta^{18}O(H_2O)$ values varied between −0.4‰ and 0.16‰, reflecting small contribution of basal meltwater and significantly less compared to mAIW (Figs. 5i and 6).

5. Discussion

In our study, we trace the CH_4 pathways within the water masses on the NEG continental shelf. The expedition took place from 12 September to October 14, 2017, i.e., after the melt peak at the summer-autumn transition when sea ice, land-fast ice and glacier melt, had discharged the largest amounts of meltwater into the upper part of PSW. Furthermore, induced by the prominent trough system, mixing between certain waters masses occur along the anti-cyclonic circulation on the NEG continental shelf. The modification of the water mass properties on the shelf eventually also affected the CH_4 pathways related to water mass origins and history. From the ocean surface to bottom depths, we found distinctive water masses on the shelf: i) PSW formed on the NEG continental shelf, ii) KW exported from the Arctic Ocean, iii) mAIW formed by a mixture between transported AIW and local meltwater from basal glacial melt and subglacial runoff, and iv) AIW originated mainly from the recirculating Atlantic waters in Fram Strait. Considering that PSW and mAIW are formed locally on the shelf, while KW and AIW are transported onto the shelf, we can distinguish processes modifying the CH_4 signal that occurred in the inner shelf from those occurred off shelf. Hence, by using the CH_4 concentration, saturation and $\delta^{13}C$, as well as $\delta^{18}O(H_2O)$, we can follow the CH_4 pathways on the NEG continental shelf.

5.1. Methane excess in water masses influenced by sea ice formation and melt

Three water masses are clearly CH_4 super-saturated (i.e., show a CH_4 excess) relative to the atmospheric equilibrium concentration (Fig. 5): MWL and WML (which form locally on the shelf), and KW (which is exported from the Arctic Ocean). WML and KW are influenced by brine release during sea ice formation in their respective formation regions (Figs. 5g and 7a; Budéus and Schneider, 1995; Huhn et al., 2021). In addition, MWL, WML and KW are localised within the water masses on the shelf without direct contact with the seafloor. Hence, we consider CH_4 sourcing from the sediment unlikely for the CH_4 excess observed in MWL, WML and KW. Moreover, unlike previous reports of CH_4 super-saturation in runoff of land-terminating glaciers (Christiansen and Jørgensen, 2018; Lamarche-Gagnon et al., 2019), no evidence for subglacial CH_4 is found (see Sect. 5.2.2). We suggest instead that this CH_4 excess is sea ice-sourced. CH_4 excess in sea ice influenced water occurs by CH_4 discharge during brine release in winter (Damm et al., 2015). The negative fraction of sea ice meltwater (f_{sim}) in WML and KW indicates brine release into these water masses and the preservation of this signal during the summer melt season (Fig. 7a). This evidence also reflects the preservation of a CH_4 excess pool (MEP) relative to the atmosphere within WML, i.e., the MEP is sustained also in summer (Figs. 4 and 9). In addition to water-side preconditions for the preservation of an MEP in summer, the enduring disconnection of both water masses from the atmosphere facilitates a long-lasting storage of a MEP in WML and KW. Deviations in the $\delta^{13}C$ values of the MEP compared to the atmospheric background $\delta^{13}C$ values, reflect the disconnection between the atmosphere and shelf water and point to an inhibited gas exchange at the sea-air interface (Fig. 4). In comparison, the deviations in $\delta^{13}C$ values between the MEP in WML and KW are related to the different formation of both water masses. The KW $\delta^{13}C$ value is higher than the WML value (Fig. 4), presumably due to ongoing microbial CH_4 oxidation during the journey of KW from the Arctic Ocean towards the NEG continental shelf. The effect of CH_4 oxidation on the residual CH_4 pool is discussed in Sect. 5.2.1. The MEP remains preserved in WML and KW. However, modifications on the MEP were observed which we link to mixing with the other surrounding water masses present on the shelf. For tracing the CH_4 pathways and the ultimate fate of CH_4, we next discuss the MEP within these surrounding water masses and the mixing processes modifying this MEP on the shelf.

5.1.1. Methane excess pool sustained in the MWL by freshwater discharge

The influence of ice melt, surface runoff from the glacier, submarine melting icebergs, glacier front melting, and subglacial runoff from the 79NG and ZI, resulted in freshening of the upper part of PSW (Figs. 2 and 3). The lower $\delta^{18}O$ value of MWL water relative to WML clearly reveals the influence of meteoric water and a slight excess of sea ice melt (Figs. 6, 7a and 7b). Remarkably, MWL remains super-saturated in CH_4, relative to the atmospheric equilibrium concentration. The sustained CH_4 excess in MWL water can be attributed to mechanisms involving both sea ice cycles and glacier melting. In summer, freshwater depleted in CH_4 from melting sea ice is added into the ocean, diluting the remaining CH_4 excess in the upper part of the WML, i.e., CH_4 excess diminishes in the seasonally formed MWL. This scenario can be observed in stations with CH_4 concentrations <4.2 nmol L^{-1} on the Norske

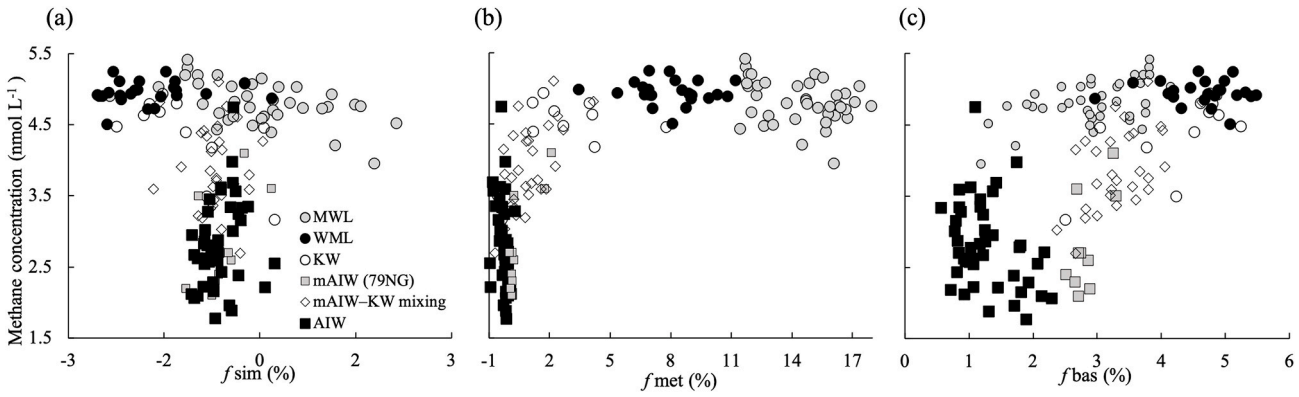

Fig. 7. CH_4 concentrations over sea ice meltwater fraction (f_{sim}), meteoric water fraction (f_{met}), and basal meltwater fraction (f_{bas}) based on a quaternary mixing between Atlantic Intermediate Water, basal meltwater, sea ice meltwater and meteoric water (see Table 1). (a) Decreasing sea ice meltwater fraction in WML and KW indicates enhanced brine released during sea ice formation and corroborates sea ice as a source for the CH_4 concentration enhancement. (b) In MWL, the increasing meteoric water fraction coupled to reduced CH_4 concentration show mixing with glacial meltwater discharge. (c) basal meltwater additions to mAIW keep CH_4 concentrations at constant values, in comparison to AIW. MWL: Meltwater Layer, WML: Winter Mixed Layer, KW: Knee Water, mAIW: modified Atlantic Intermediate Water, and AIW: Atlantic Intermediate Water.

Trough (Fig. 5d). There, a higher contribution of freshwater from melting sea ice in comparison to freshwater of glacial origin is expected to occur, due to the northward circulation pattern moving meltwater of glacial origin toward the north (Fig. 3). Although we lack $\delta^{18}O$ observations in stations on the Norske Trough, the concentrations of CH_4 below the saturation (equilibrium) concentration suggest dilution by sea ice melt as a process favoring CH_4 redistribution in the marine environment. By contrast, the MWL CH_4 concentration is marginally lower than the WML (by about 0.1 nmol L^{-1}) in stations on the inner shelf (ZI), 79NG, and Dijmphna Sund (Fig. 5). Presumably, due to melting of pre-Holocene ice, with equivalent CH_4 concentrations as low as 1.8 nmol L^{-1} (Baumgartner et al., 2014). However, this meltwater may equilibrate with the atmosphere on their way to the ocean (as surface run-off, Fig. 2b and 2c). This is reflected by the apparent meltwater CH_4 concentration of about (4.0 ± 0.5) nmol L^{-1} that can be calculated by extrapolating to $S = 0$. The decreasing $\delta^{13}C$ values with increasing f_{met} (to −48‰ for f_{met} = 17%) further supports our hypothesis that the meltwater equilibrates with the atmosphere (data not shown). Finally, the lid effect of freshwater discharge of various origins set up a stable water column stratification and reduced the vertical mixing (Fig. 4c). Both favoured the storage of the remaining CH_4 excess (Damm et al., 2015; Verdugo et al., 2021). MWL O_2 is undersaturated by 3–6% (data not shown) and corroborates our assumption that gas exchange is slow enough for the CH_4 super-saturation to persist as well (Fig. 5e). Hence, the meltwater slightly diluted the MEP and inhibited the efflux from the NEG continental shelf waters to the atmosphere, due to increased stratification.

5.1.2. Methane excess pool in KW diluted by mixing with mAIW

Tracing the fate of the MEP formed in KW, we followed this water mass from the calving front of the 79NG where the floating glacier tongue is about 100 m thick toward Westwind Trough. MAIW exits the glacier cavity and mixes with KW both covering the same density classes (Figs. 3 and 6). We suggest that the mixing of both water masses continues in the Westwind Trough. There, a higher fraction of brine-enriched KW has been reported (Budéus and Schneider, 1995). Mixing between KW and mAIW induces enhanced CH_4 concentration at the transition zone between both water masses, with KW as source of the CH_4 excess (Fig. 5e). Moreover, the negative sea ice meltwater fractions reflect the mixture between the sea ice-influenced KW and mAIW that is far less influenced by sea ice formation (Figs. 5g and 7a). Additionally, the heterogeneous $\delta^{13}C$ values corroborate effective mixing as a process resulting in distributing CH_4 from KW into mAIW (Fig. 4).

5.2. Dissolved methane in water masses uninfluenced by sea ice formation and melt

5.2.1. Methane oxidation detected in AIW on the NEG continental shelf

On the shelf, AIW is localised below mAIW and KW (Fig. 3). In AIW, we found CH_4 under-saturation, while AIW $\delta^{13}C$ value was higher than for PSW (Fig. 4). AIW is transported from Fram Strait via Norske Trough towards the inner shelf for about 24 days (Hattermann et al., 2016) at depth remaining unaffected by sea ice formation. Still, as this water mass is in direct contact with the seafloor on the shelf, we are tracing the CH_4 pathway backward to detect potential impacts of sediment-released CH_4. Both aspects, the CH_4 under-saturation and the enrichment in ^{13}C reflect CH_4 oxidation during long-term water mass journey (Damm et al., 2005; Valentine et al., 2001). To apply and investigate this assumption on the NEG shelf, we calculated potential CH_4 oxidation occurring during the long-term AIW journey (from Fram Strait toward the shelf break) using the CH_4 concentrations and the $\delta^{13}C$ values in the supra-bottom and bottom layer with σ_θ between 27.8 and 27.89 kg m^{-3} and $\sigma_\theta > 27.89$ kg m^{-3}, respectively.

We calculated a Rayleigh fractionation curve (RC) following Eq. (5):

$$\ln(1+\delta) = \ln(1+\delta_0) + \left(\frac{1}{\alpha} - 1\right)\ln f \quad (5)$$

α is the isotopic fractionation factor, f is the fraction of residual CH_4 in AIW, and δ_0 corresponds to the $\delta^{13}C$ of CH_4 at 78.153° N, 0.008° E, which we used as source signal from the Fram Strait (Fig. 8). We used these values as most likely to represent the potential pool that is going to be oxidised within this water mass. Assuming CH_4 oxidation, the RC shows that AIW entered the shelf with threshold CH_4 values down to 2.2 nmol L^{-1}. Threshold values are reached when CH_4 oxidation ceased due to substrate limitation, preventing further microbial oxidation of CH_4 (Scranton and Brewer, 1978; Valentine et al., 2001). In addition, the residual CH_4 pool is enriched in ^{13}C, compared to the CH_4 pool before CH_4 consumption occurred (Fig. 8). Moreover, the enrichment in ^{13}C in the bottom layer, relative to the $\delta^{13}C$ values in the supra-bottom layer, reflects the different CH_4 oxidation efficiency between both layers. The supra-bottom layer values scatter around RC1 calculated with $\alpha = 1.003$, while the bottom layer values partly scatter around RC1, and partly around a second RC (RC2) with a higher $\alpha = 1.015$ (Fig. 8). Both α values are within the range of values determined for Arctic shelf waters (Damm et al., 2005, 2007). Favoured CH_4 consumption in the bottom layer is probably induced by high bottom-intensified velocities resuspending microbes at the sediment-water interface (Murrell, 2010) and consequently transported with the bottom layer.

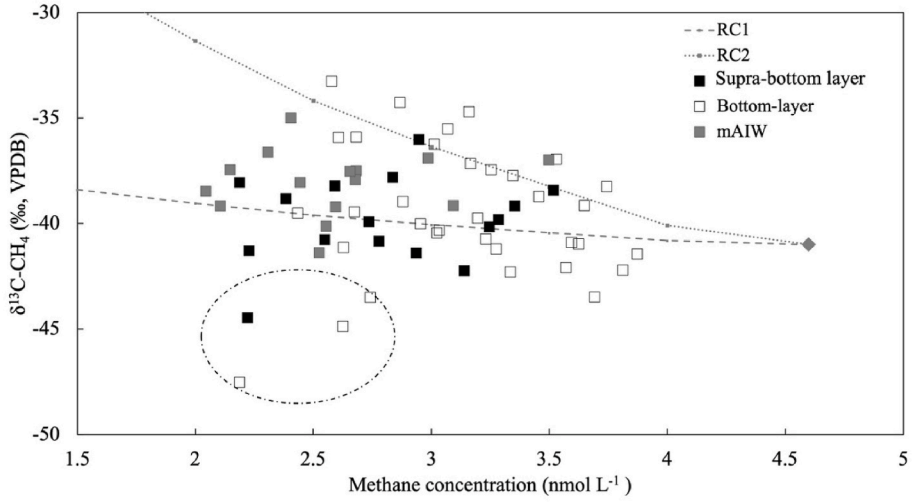

Fig. 8. CH_4 concentration versus the $\delta^{13}C$ in the supra-bottom and bottom layer of the Atlantic Intermediate Water (AIW) combined with two calculated Rayleigh oxidation curves (RC). Grey diamond represents the initial CH_4 (source) from station 5 in Fram Strait (78.153° N, 0.008° E) that was used as the starting point for the calculated RC. The values from the supra-bottom layer and bottom layer scatter around RC1 and RC2 calculated with an $\alpha = 1.003$ and 1.015, respectively (see Sect. 5.2.1). Oxidation occurred during AIW journey from Fram Strait to the shelf break. At the inner shelf, AIW contains an oxidised threshold CH_4 pool with values down to 2.2 nmol L^{-1}. The oxidised threshold CH_4 pool remains sustained in mAIW, as the basal meltwater contains similar CH_4 concentrations than those found in AIW. Circled samples from the shelf bottom deviated from both RC reflecting the influence of additional processes.

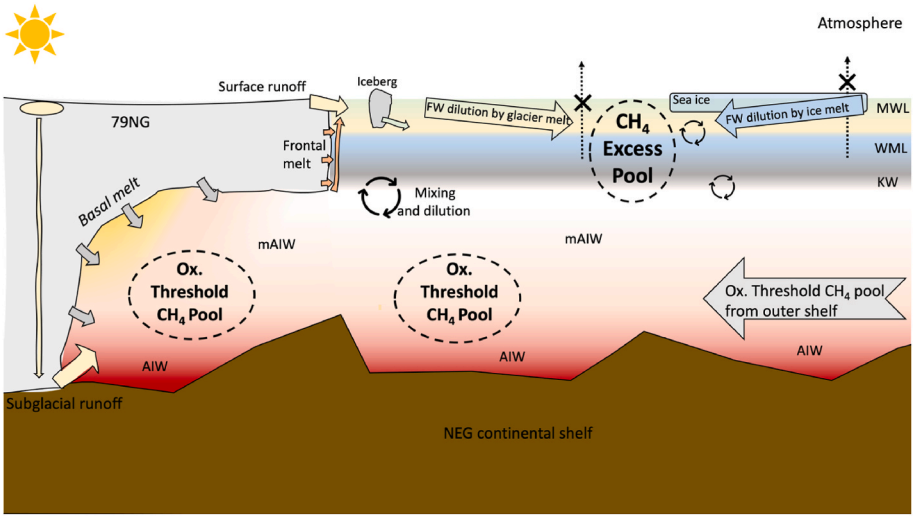

Fig. 9. Sketch indicating CH_4 pathways related to the water masses and meltwaters on the NEG continental shelf during the summer-autumn transition. In the upper water column, the methane excess pool (MEP) is localised in the winter mixed layer (WML) and Knee Water (KW). The MEP remains sustained as the formation of a meltwater layer (MWL) inhibits the sea-to-air flux via increased stratification. Surface runoff from the glacier (yellow arrow), submarine melting from icebergs (green arrow), subglacial runoff (carried with a meltwater plume along the glacier base to shallower depths), frontal melting (orange arrows), and the melting sea ice (blue arrow) contribute to the formation of a freshwater lid that restricts the exchange of CH_4 between the ocean surface and the atmosphere (black arrow overlaid with a cross). Deeper water column: An oxidised (Ox.) threshold CH_4 pool is present at the continental shelf break, i.e., threshold concentration preventing further microbial oxidation of CH_4. Once on the shelf, the oxidised threshold CH_4 pool is transported by the Atlantic Intermediate Water (AIW). In the glacier cavity, AIW is mixed with the basal meltwater discharged from the glacier (and the subglacial runoff) and forms the modified AIW (mAIW). The oxidised threshold CH_4 pool remains sustained in mAIW, as the basal meltwater contains similar CH_4 concentrations than those found in AIW. The basal meltwater discharged into mAIW does not have a significant effect on its CH_4 concentration but enables the incorporation of CH_4 from additions of KW. Mixing and dilution are shown by circled arrows. FW = freshwater.

When AIW reached the inner shelf, CH_4 consumption has reduced the CH_4 concentration to about 57% relative to the values in the Fram Strait. Hence, we conclude CH_4 oxidation is an efficient process for the consumption of CH_4 within AIW outer shelf, and that AIW as a source of CH_4 for the shelf waters can be dismissed.

In summary, both PSW and AIW can be well distinguished in terms of their CH_4 signal and the process influencing the CH_4 pathways in both water masses (Fig. 9). In the following, we used the oxidised threshold CH_4 pool in AIW on the shelf (as initial reference) to trace if the discharged glacial meltwater acts as a source for CH_4 on the shelf.

5.2.2. *Methane in glacially modified AIW (mAIW)*

Propagating from the inner shelf, AIW enters the 79NG cavity with oxidised CH_4 threshold values (Figs. 8 and 9). In the cavity, the glacial basal melt is induced by the heat derived from AIW (Schaffer et al., 2017; Wilson and Straneo, 2015), leading to the formation of mAIW. Hence, AIW with the oxidised CH_4 threshold is mixed with the discharged glacial meltwater. Thereafter, the newly formed mAIW is transported out of the cavity via an overturning circulation induced by the glacial cavity bathymetry. The discharged glacial meltwater on mAIW is clearly shown by the light $\delta^{18}O$ signature of mAIW relative to AIW (Fig. 6). We attribute the change from AIW to mAIW to an addition of 4.5% of basal meltwater. Moreover, estimating the CH_4 concentrations in basal meltwater using a CH_4 mole fraction of between 0.5 (LGM) and 0.75 μmol mol^{-1} (Eemian) and an air concentration in ice of 0.09 cm^3 g^{-1} (Baumgartner et al., 2014) results in concentrations between 1.8 and 2.8 nmol L^{-1}. The similar CH_4 concentrations in both basal meltwater and AIW (Figs. 4 and 7c) are indicative that the added basal meltwater does not change the mAIW CH_4 concentration. Even though we observed only a small basal meltwater contribution in mAIW, we therefore conclude that the discharged glacial meltwater from these marine-terminating glaciers does not act as a source of CH_4 for mAIW, i.e., we are also able to rule out a glacial meltwater source on the enhanced CH_4 concentrations in surface waters. The similar $\delta^{13}C$ of CH_4 in both water masses (mAIW and AIW) further corroborates that the glacial meltwater discharge as a source of CH_4 for mAIW can be dismissed (Figs. 4 and 7c).

Furthermore, tracing the mixing of AIW and the discharged glacial

meltwater, we followed the further CH_4 pathways within mAIW. As shown in section 5.1.2, CH_4 in mAIW is mixed with KW, as observed in the enhanced CH_4 concentrations at the interface of both water masses in the Westwind Trough (Fig. 5d). Hence, sea ice-sourced CH_4 contained within KW is incorporated into mAIW, i.e., the basal meltwater discharged into the shelf waters dilutes the CH_4 excess in KW. In summary, we infer that (i) the CH_4 excess in shelf waters is sea ice-sourced, and (ii) this CH_4 excess is redistributed in the marine environment. A mixture of different meltwater types contributes to the formation of a freshwater lid that restricts the sea-to-air flux via increased water column stratification, while basal meltwater marginally dilutes the MEP at the interface between KW and mAIW (Fig. 9).

6. Conclusions

At the NEG continental shelf, CH_4 excess is detected in water masses interacting with sea ice. The CH_4 excess in WML and KW is thought to be induced by brine release during sea ice formation. The freshwater discharge from glacier and sea ice melting forms a freshwater lid, which restricts the sea-to-air flux and contributes to the sustainment of a CH_4 excess in the MWL and WML underneath via increased stratification (Fig. 9). This implies that the CH_4 excess remains stored on the NEG continental shelf waters, i.e., in the marine environment. In water masses not affected by sea ice (mAIW and AIW) oxidised CH_4 threshold values are detected. Those CH_4 concentrations are induced by CH_4 oxidation shown by the ^{13}C-enriched values within the AIW before reaching the inner shelf. Hence, both water masses act as a microbiological CH_4 sink. The basal meltwater discharged into mAIW does not have a significant effect on its CH_4 concentration but enables the incorporation of CH_4 from additions of KW. Modelling studies that include interactions between sea ice processes, ocean, and glaciers are needed to determine the long-term effects on the methane sources and sinks balance in Arctic shelf waters.

Authors contribution

J.V. wrote the manuscript. J.V. and E.D. designed the study and carried out the geochemical analyses, J.S. the oceanographic analysis, D. B. the water mass tracer analysis, J.K. the water mass fraction analysis, and H.M. measured the $\delta^{18}O(H_2O)$ samples. All authors contributed to the interpretation of the data, and to the manuscript text and figures.

Declaration of competing interest

The authors declare that they have no known competing financial interests or personal relationships that could have appeared to influence the work reported in this paper.

Data availability

CTD data are available at https://doi.pangaea.de/10.1594/PANGAEA.883366 and Biogeochemical data will be available at Pangaea.de

Acknowledgment

We sincerely acknowledge the support of the captain and crew of R/V *Polarstern* cruise PS109 for their professional support at sea. We thank Ilsetraut Stölting for her support on the methane samples analyses. This study was funded through the Alfred-Wegener-Institute, Helmhotz-Zentrum für Polar und Meeresforschung. Expedition grant number AWI_PS109_03. J.V. received a scholarship from the National Agency for Research and Development (ANID)/Scholarship Program/Becas de Doctorado con acuerdo bilateral en el extranjero CONICYT-DAAD/2016–62150023. German Academic Exchange Service (DAAD) reference number 91609942. J.S. acknowledges support from the German Federal Ministry for Education and Research (BMBF) within the GROCE project (grant 03F0778A). Sea ice concentration data from September 20, 2017 were obtained from https://www.meereisportal.de (grant: REKLIM-2013-04).

References

Arndt, J.E., Jokat, W., Dorschel, B., Myklebust, R., Dowdeswell, J.A., Evans, J., 2015. A new bathymetry of the Northeast Greenland continental shelf: constraints on glacial and other processes. G-cubed 16, 3733–3753. https://doi.org/10.1002/2015GC005931.

Bauch, D., Hölemann, J., Andersen, N., Dobrotina, E., Nikulina, A., Kassens, H., 2010. The Arctic shelf regions as a source of freshwater and brine-enriched waters as revealed from stable oxygen isotopes. Polarforschung 80, 127–140.

Bauch, D., Schlosser, P., Fairbanks, R.G., 1995. Fresh-water balance and the sources of deep and bottom waters in the arctic-ocean inferred from the distribution of (H20)-O- 18. Prog. Oceanogr. 35, 53–80. https://doi.org/10.1016/0079-6611(95)00005-2.

Baumgartner, M., Kindler, P., Eicher, O., Floch, G., Schilt, A., Schwander, J., Spahni, R., Capron, E., Chappellaz, J., Leuenberger, M., Fischer, H., Stocker, T.F., 2014. NGRIP CH4 concentration from 120 to 10 kyr before present and its relation to a δ15N temperature reconstruction from the same ice core. Clim. Past 10, 903–920. https://doi.org/10.5194/cp-10-903-2014.

Bourke, R.H., Newton, J.L., Paquette, R.G., Tunnicliffe, M.D., 1987. Circulation and water masses of the East Greenland shelf. J. Geophys. Res. 92, 6729. https://doi.org/10.1029/JC092iC07p06729.

Budéus, G., Schneider, W., 1995. On the generation of The Northeast water polynya. J. Geophys. Res. 100, 4269. https://doi.org/10.1029/94JC02349.

Christiansen, J.R., Jørgensen, C.J., 2018. First observation of direct methane emission to the atmosphere from the subglacial domain of the Greenland Ice Sheet. Sci. Rep. 8, 2–7. https://doi.org/10.1038/s41598-018-35054-7.

Crabeck, O., Delille, B., Thomas, D., Geilfus, N.X., Rysgaard, S., Tison, J.L., 2014. CO2 and CH4 in sea ice from a subarctic fjord under influence of riverine input. Biogeosciences 11, 6525–6538. https://doi.org/10.5194/bg-11-6525-2014.

Damm, E., Bauch, D., Krumpen, T., Rabe, B., Korhonen, M., Vinogradova, E., Uhlig, C., 2018. The transpolar drift conveys methane from the siberian shelf to the central Arctic Ocean. Sci. Rep. 8, 4515. https://doi.org/10.1038/s41598-018-22801-z.

Damm, E., Ericson, Y., Falck, E., 2021. Waterside convection and stratification control methane spreading in supersaturated Arctic fjords (Spitsbergen). Continent. Shelf Res. 224, 104473 https://doi.org/10.1016/j.csr.2021.104473.

Damm, E., Mackensen, A., Budéus, G., Faber, E., Hanfland, C., 2005. Pathways of methane in seawater: plume spreading in an Arctic shelf environment (SW-Spitsbergen). Continent. Shelf Res. 25, 1453–1472. https://doi.org/10.1016/j.csr.2005.03.003.

Damm, E., Rudels, B., Schauer, U., Mau, S., Dieckmann, G., 2015. Methane excess in Arctic surface water-triggered by sea ice formation and melting. Sci. Rep. 5, 16179. https://doi.org/10.1038/srep16179.

Damm, E., Schauer, U., Rudels, B., Haas, C., 2007. Excess of bottom-released methane in an Arctic shelf sea polynya in winter. Continent. Shelf Res. 27, 1692–1701. https://doi.org/10.1016/j.csr.2007.02.003.

Ekwurzel, B., Schlosser, P., Mortlock, R.A., Fairbanks, R.G., Swift, J.H., 2001. River runoff, sea ice meltwater, and Pacific water distribution and mean residence times in the Arctic Ocean. J. Geophys. Res.: Oceans 106, 9075–9092. https://doi.org/10.1029/1999JC000024.

Enderlin, E.M., Hamilton, G.S., Straneo, F., Sutherland, D.A., 2016. Iceberg meltwater fluxes dominate the freshwater budget in Greenland's iceberg-congested glacial fjords. Geophys. Res. Lett. 43 (11), 287. https://doi.org/10.1002/2016GL070718, 11,294.

Fuex, A.N., 1980. Experimental evidence against an appreciable isotopic fractionation of methane during migration. Phys. Chem. Earth 12, 725–732. https://doi.org/10.1016/0079-1946(79)90153-8.

Gentz, T., Damm, E., Schneider von Deimling, J., Mau, S., McGinnis, D.F., Schlüter, M., 2014. A water column study of methane around gas flares located at the West Spitsbergen continental margin. Continent. Shelf Res. 72, 107–118. https://doi.org/10.1016/j.csr.2013.07.013.

Gill, A.E., 1982. Atmosphere-Ocean Dynamics. Elsevier Science.

Hattermann, T., Isachsen, P.E., Von Appen, W.J., Albretsen, J., Sundfjord, A., 2016. Eddy-driven recirculation of atlantic water in Fram Strait. Geophys. Res. Lett. 43, 3406–3414. https://doi.org/10.1002/2016GL068323.

Huhn, O., Rhein, M., Kanzow, T., Schaffer, J., Sültenfuß, J., 2021. Submarine meltwater from nioghalvfjerdsbræ (79 north glacier), northeast Greenland. J. Geophys. Res.: Oceans 1–17. https://doi.org/10.1029/2021jc017224.

IPCC, 2021. Summary for policymakers. In: Climate Change 2021: the Physical Science Basis. Contribution of Working Group I to the Sixth Assessment Report of the Intergovernmental Panel on Climate Change. Cambridge University Press (in press).

Kanzow, T., Rohardt, G., 2017. CTD raw data files from POLARSTERN cruise PS109, link to tar-archive. In: Rohardt, Gerd (Ed.), Archive of CTD Raw Data Files of POLARSTERN Cruises. Alfred Wegener Institute, Helmholtz Centre for Polar and Marine Research, Bremerhaven, PANGAEA. https://doi.org/10.1594/PANGAEA.883366, 2017 10.1594/PANGAEA.852715.

Kitidis, V., Upstill-Goddard, R.C., Anderson, L.G., 2010. Methane and nitrous oxide in surface water along The north-west passage, Arctic Ocean. Mar. Chem. 121, 80–86. https://doi.org/10.1016/j.marchem.2010.03.006.

Kwok, R., 2018. Arctic sea ice thickness, volume, and multiyear ice coverage: losses and coupled variability (1958-2018). Environ. Res. Lett. 13 https://doi.org/10.1088/1748-9326/aae3ec.

Lamarche-Gagnon, G., Wadham, J.L., Sherwood Lollar, B., Arndt, S., Fietzek, P., Beaton, A.D., Tedstone, A.J., Telling, J., Bagshaw, E.A., Hawkings, J.R., Kohler, T.J., Zarsky, J.D., Mowlem, M.C., Anesio, A.M., Stibal, M., 2019. Greenland melt drives continuous export of methane from the ice-sheet bed. Nature 565, 73–77. https://doi.org/10.1038/s41586-018-0800-0.

Mankoff, K.D., Straneo, F., Cenedese, C., Das, S.B., Richards, C.G., Singh, H., 2016. Structure and dynamics of a subglacial discharge plume in a Greenlandic fjord. J. Geophys. Res.: Oceans 121, 8670–8688. https://doi.org/10.1002/2016JC011764.

Mau, S., Blees, J., Helmke, E., Niemann, H., Damm, E., 2013. Vertical distribution of methane oxidation and methanotrophic response to elevated methane concentrations in stratified waters of the Arctic fjord Storfjorden (Svalbard, Norway). Biogeosciences 10, 6267–6268. https://doi.org/10.5194/bg-10-6267-2013.

Mau, S., Römer, M., Torres, M.E., Bussmann, I., Pape, T., Damm, E., Geprägs, P., Wintersteller, P., Hsu, C.-W., Loher, M., Bohrmann, G., 2017. Widespread methane seepage along the continental margin off Svalbard - from Bjørnøya to Kongsfjorden. Sci. Rep. 7, 42997. https://doi.org/10.1038/srep42997.

Mayer, C., Reeh, N., Jung-Rothenhäusler, F., Huybrechts, P., Oerter, H., 2000. The subglacial cavity and implied dynamics under Nioghalvfjerdsfjorden Glacier, NE-Greenland. Geophys. Res. Lett. 27, 2289–2292. https://doi.org/10.1029/2000GL011514.

Meyer, H., Schönicke, L., Wand, U., Hubberten, H.W., Friedrichsen, H., 2000. Isotope studies of hydrogen and oxygen in ground ice - experiences with the equilibration technique. Isot. Environ. Health Stud. 36, 133–149. https://doi.org/10.1080/10256010008032939.

Mouginot, J., Rignot, E., Scheuchl, B., Fenty, I., Khazendar, A., Morlighem, M., Buzzi, A., Paden, J., 2015. Fast retreat of Zachariae isstrom, northeast Greenland. Science 350, 1357–1361. https://doi.org/10.1126/science.aac7111, 1979.

Murrell, J.C., 2010. The aerobic methane oxidizing bacteria (Methanotrophs). In: Timmis, K.N. (Ed.), Handbook of Hydrocarbon and Lipid Microbiology. Springer, Berlin, Heidelberg, pp. 1953–1966. https://doi.org/10.1007/978-3-540-77587-4.

Parmentier, F.-J.W., Christensen, T.R., Sørensen, L.L., Rysgaard, S., McGuire, a.D., Miller, P.a., Walker, D.a., 2013. The impact of lower sea-ice extent on Arctic greenhouse-gas exchange. Nat. Clim. Change 3, 195–202. https://doi.org/10.1038/nclimate1784.

Perovich, D., Meier, W., Tschudi, M., Hendricks, S., Petty, A.A., Divine, D., Farrell, S., Gerland, S., Haas, C., Kaleschke, L., Pavlova, O., Richer, R., Tian-Kunze, X., Webster, M., Wood, K., 2020. Sea Ice. https://doi.org/10.25923/n170-9h57 [WWW Document].

Rignot, E., Mouginot, J., 2012. Ice flow in Greenland for the international polar year 2008-2009. Geophys. Res. Lett. 39, 1–7. https://doi.org/10.1029/2012GL051634.

Rohardt, G., 2017. Archive of CTD Raw Data Files of POLARSTERN Cruises. Bremerhaven, Germany. https://doi.org/10.1594/PANGAEA.852715.

Schaffer, J., Kanzow, T., von Appen, W.J., von Albedyll, L., Arndt, J.E., Roberts, D.H., 2020. Bathymetry constrains ocean heat supply to Greenland's largest glacier tongue. Nat. Geosci. 13 https://doi.org/10.1038/s41561-019-0529-x.

Schaffer, J., von Appen, W.J., Dodd, P.A., Hofstede, C., Mayer, C., de Steur, L., Kanzow, T., 2017. Warm water pathways toward Nioghalvfjerdsfjorden glacier, northeast Greenland. J. Geophys. Res.: Oceans 122, 4004–4020. https://doi.org/10.1002/2016JC012462.

Schlitzer, R., 2020. Ocean Data View.

Scranton, M.I., Brewer, P.G., 1978. Consumption in the deep ocean1. Sci. N. Y. 23, 1207–1213.

Silyakova, A., Jansson, P., Serov, P., Ferré, B., Pavlov, A.K., Hattermann, T., Graves, C.A., Platt, S.M., Myhre, C.L., Gründger, F., Niemann, H., 2020. Physical controls of dynamics of methane venting from a shallow seep area west of Svalbard. Continent. Shelf Res. 194, 104030 https://doi.org/10.1016/j.csr.2019.104030.

Sneed, W.A., Hamilton, G.S., 2016. Recent changes in the Norske oer ice barrier, coastal northeast Greenland. Ann. Glaciol. 57, 47–55. https://doi.org/10.1017/aog.2016.21.

Spreen, G., Kaleschke, L., Heygster, G., 2008. Sea Ice Remote Sensing Using AMSR-E 89-GHz Channels 113, pp. 1–14. https://doi.org/10.1029/2005JC003384.

Stroeve, J., Notz, D., 2018. Changing state of Arctic sea ice across all seasons. Environ. Res. Lett. 13, 103001 https://doi.org/10.1088/1748-9326/aade56.

Valentine, D.L., Blanton, D.C., Reeburgh, W.S., Kastner, M., 2001. Water column methane oxidation adjacent to an area of active hydrate dissociation, Eel River Basin. Geochem. Cosmochim. Acta 65, 2633–2640. https://doi.org/10.1016/S0016-7037(01)00625-1.

Verdugo, J., Damm, E., Nikolopoulos, A., 2021. Methane cycling within sea ice: results from drifting ice during late spring, north of Svalbard. Cryosphere 15, 2701–2717. https://doi.org/10.5194/tc-15-2701-2021.

White, J.W.C., Vaughn, B.H., Michel, S.E., 2018. Stable Isotopic Composition of Atmospheric Methane (13C) from the NOAA ESRL Carbon Cycle Cooperative Global Air Sampling Network, 1998-2017. Version: 2018-09-24.

Wiesenburg, D.A., Guinasso Jr., N.L., 1979. Equilibrium solubilities of methane, carbon monoxide, and hydrogen in water and sea water. Section Title: Water 24, 356–360. https://doi.org/10.1021/je60083a006.

Wilson, N., Straneo, F., Heimbach, P., 2017. Satellite-derived submarine melt rates and mass balance (2011–2015) for Greenland's largest remaining ice tongues. Cryosphere 11, 2773–2782. https://doi.org/10.5194/tc-11-2773-2017.

Wilson, N.J., Straneo, F., 2015. Water exchange between the continental shelf and the cavity beneath Nioghalvfjerdsbrae (79 North Glacier). Geophys. Res. Lett. 42, 7648–7654. https://doi.org/10.1002/2015GL064944.